Cellular and Molecular Life Sciences (2022) 79:354
https://doi.org/10.1007/s00018-022-04385-0

ORIGINAL ARTICLE

The protective effect of selenoprotein M on non-alcoholic fatty liver disease: the role of the AMPKα1–MFN2 pathway and Parkin mitophagy

Jingzeng Cai[1] · Jiaqiang Huang[2] · Jie Yang[1] · Xiaoming Chen[1] · Haoran Zhang[1] · Yue Zhu[1] · Qi Liu[1] · Ziwei Zhang[1,3]

Received: 24 January 2022 / Revised: 4 May 2022 / Accepted: 19 May 2022 / Published online: 9 June 2022

Abstract

Non-alcoholic fatty liver disease (NAFLD) is related to a dysregulation of mitophagy, a process that is not fully understood. *Parkin*-related mitophagy can sustain mitochondrial homeostasis and hepatocyte viability. Herein, we report that selenoprotein M (SELENOM) plays a central role in maintaining mitophagy in high-fat diet (HFD)-mediated NAFLD. We show that SELENOM was significantly downregulated in the liver of HFD-fed mice. SELENOM deletion aggravated HFD-mediated hepatic steatosis, inflammation, and fibrosis; accompanied by enhanced fatty acid oxidation and oxidative stress in the liver. Molecular analyses show that lipotoxicity was related to increased mitochondrial apoptosis as evidenced by enhanced mitochondrial ROS production, and attenuation of mitochondrial potential in the liver of HFD-fed SELENOM$^{-/-}$ mice. Additionally, SELENOM deletion reduced mitophagy and aggravated hepatic injury in NAFLD. Mechanistically, SELENOM overexpression activated *Parkin*-mediated mitophagy to reduce mitochondrial apoptosis and remove HFD-damaged mitochondria. We further found that SELENOM regulates *Parkin* expression via the AMPKα1–MFN2 pathway; blockade of AMPKα1 prevented SELENOM activation of *Parkin*-mediated mitophagy. Our work identified SELENOM downregulation as a possible explanation for the defective mitophagy in NAFLD. Thus, targeting SELENOM may be potential new therapeutic modalities for NAFLD treatment.

Keywords SELENOM · NAFLD · Mitochondria homeostasis · Oxidative stress · Mitophagy

Introduction

Selenoproteins have important regulatory effects on fatty liver and lipid metabolism. Selenoprotein P is involved in the pathogenesis of non-alcoholic fatty liver disease (NAFLD) by regulating lipid accumulation [1]. Hepatic selenoprotein S deficiency caused hepatic steatosis and insulin resistance via regulating hepatic lipid accumulation and insulin action [2]. Selenoprotein M (SELENOM) is one of the selenoproteins in the selenoprotein family. SELENOM, a key thioredoxin-like enzyme present in the endoplasmic reticulum (ER), has been associated with hepatocellular degeneration and carcinoma [3, 4]. SELENOM exerts its physiological effects in many pathways including redox control, fatty acid composition, stress response and cancer cell proliferation [5, 6]. SELENOM could increase antioxidant activity to reduce the levels of oxidative and mitochondria stress in the progression of Alzheimer's disease [7]. Recent data showed that SELENOM is involved in redox signaling and energy metabolism through regulating *STAT3* phosphorylation and cytosolic calcium responses [5, 8]. In addition, SELENOM has roles in the regulation of ER and inflammatory stress responses to ameliorate metabolic dysfunction [5, 9]. In liver diseases, selenoproteins have been reported to inhibit oxidative damage and imbalance of mitochondrial dynamic in response to several types of stress [10–12]. Loss of SELENOM could increase obesity by affecting metabolic and endocrine functions [13]. Therefore, SELENOM may be

✉ Ziwei Zhang
zhangziwei@neau.edu.cn

1 College of Veterinary Medicine, Northeast Agricultural University, Harbin 150030, People's Republic of China

2 Beijing Advanced Innovation Center for Food Nutrition and Human Health, Department of Nutrition and Health, China Agricultural University, Beijing 100083, People's Republic of China

3 Department of Heilongjiang for Common Animal Disease Prevention and Treatment, Key Laboratory of the Provincial Education, Harbin, People's Republic of China

able to alleviate disorders of lipid metabolism and high-fat diet (HFD)-mediated mitochondrial damage in NAFLD.

The incidence of NAFLD is expected to increase with the prevalence of obesity and diabetes globally. NAFLD is the culmination of multiple disorders, including abnormal lipid metabolism, oxidative stress, mitochondrial dysfunction, and lipid peroxidative stress [14]. HFD could contribute to NAFLD, but the mechanisms by which HFD causes excessive accumulation of lipid in hepatocytes are complex, and multiple pathological factors are involved, especially hepatic oxidative stress and mitochondrial dysfunction [15]. NAFLD is often accompanied by lipotoxicity-induced hepatocyte apoptosis and inflammatory response [16]. There is increasing evidence that alterations in the gut microbiota (dysbiosis) influence NAFLD pathological processes [17]. Mitochondrial damage contributes to NAFLD at different levels by impairing fatty liver functions, stimulate the overproduction of reactive oxygen species (ROS), which in turn triggers pro-inflammatory cytokine release, lipid peroxidation and mitochondria-dependent apoptosis to aggravate HFD-mediated liver injury [18, 19]. Thus, restoring mitochondria homeostasis is vital to reverse or retard these NAFLD processes. However, the molecular mechanisms regulating mitochondrial homeostasis for this disease remain unclear.

Mitophagy is a specific type of autophagy that targets damaged mitochondria for degradation by lysosomes in response to mitochondrial stress, to maintain a healthy mitochondrial population [20]. Liver fibrosis has been associated with excess ROS levels and inhibition of mitophagy [21, 22], and mitophagy activation is essential to protect hepatocyte function against mitochondrial apoptosis [23]. The *Parkin*-dependent mitophagy pathway, including the P62 protein-mediated ubiquitination, is involved in sustaining mitochondrial function to ameliorate HFD-induced NAFLD [24]. Defects in the PTEN-induced kinase 1 (*PINK1*) protein and *Parkin*-dependent mitophagy could exacerbate acetaminophen-induced liver injury [25]. Activation of the *PINK1/Parkin*-mediated mitophagy pathway may also involve *AMPKα1* signaling [26], and the *AMPK–MFN2* axis may be involved in regulating the mitochondrial-associated ER membrane (MAM) and mitophagy [27, 28]. Clearly, mitophagy is an important pathway in different liver defects. However, the role of mitophagy in HFD conditions and NAFLD remains largely unknown.

In this study, we show that SELENOM expression was markedly reduced in NAFLD induced by HFD in vivo, and in AML12 hepatocytes treated with palmitic acid (PA) in vitro. Although the *AMPK–MFN2* axis is involved in the mitochondrial-associated ER membrane (MAM) and autophagy regulation [27, 28], this pathway has not been shown in mitophagy regulation of NAFLD. Accordingly, our study aims to determine how SELENOM regulates the development of NAFLD via mitophagy, whether the role of SELENOM is dependent on *AMPKα1–MFN2* signaling, especially focusing on the mitochondrial apoptosis in fatty liver disease.

Methods

Animal treatment

Male SELENOM wild-type (WT) and knockout (SELENOM$^{-/-}$) C57BL/6 J mice were purchased from Cyagen Biosciences (Cyagen Inc., US). Four-week-old mice (20–25 g) were first housed for 18 weeks under standard conditions (12/12 h of light/dark cycle, 50% ± 4% humidity, 23–25 °C) in individual cages with access to food and water ad libitum. At 4 weeks of age, mice were randomly assigned to receive HFD diet for NAFLD induction, or normal chow diet for another 18 weeks, as previously reported [29]. The composition and energy density of the diets are listed in Table S1. After 18 weeks, fasting blood samples and liver specimens were collected following an overnight fast, and stored at − 80 °C. All animal studies were performed in triplicates.

Histopathological analysis

Liver tissue processing was as previously described [30]. Briefly, liver samples were fixed in 4% paraformaldehyde for 2 h at 4 °C, embedded in paraffin, sectioned at 0.2–0.3 cm and stained with hematoxylin and eosin (H&E, Gibco, USA, 008011), Masson stain or Sirius Red (Gibco, USA, 4351405). Pathological changes were observed with a Nikon optical microscope (Mitsubishi Inc., Japan, S154), and the staining intensity quantified with Image-Pro Plus 6.0 (Media Cybernetics, USA). The average diameter of hepatic vacuolations was measured by Image-Pro Plus 6.0 as previously described [31].

Biochemical evaluation

To evaluate liver injury, the levels of alanine transaminase (ALT), total cholesterol (TC), aspartate transaminase (AST) and triglyceride (TG) (Abcam, UK, ab234579 for ALT, ab282928 for TC, ab105134 for AST, ab178780 for TG) in the serum were determined with commercial kits on the automatic biochemical analyzer HITACHI 7020 (Hitachi, Tokyo, Japan, DS12556).

Transmission electron microscopy (TEM)

The liver tissues were fixed with 3% glutaraldehyde, post fixed with 1% osmium, dehydrated and embedded for ultrathin sectioning at 70 nm. Sections were stained with uranyl

acetate, lead citrate, and dried for imaging at 80 kV to detect changes in autophagy under the TEM (Elibo Biotechnology Co., Ltd, Japan, GEM-1200ES).

Cell culture and treatment

AML12 hepatocytes (ATCC, USA) were cultured in Dulbecco's modified Eagle's medium (Gibco, USA, GB12511) supplemented with 10% fetal bovine serum (FBS) at 37 °C in a humidified 5% CO_2 atmosphere to 90–100% confluence, with medium changes every 2 days. In some experiments, cells were treated with the palmitic acid (PA, 75 μM; Sigma-Aldrich, G11512) for 24 h to simulate a lipotoxicity. For AMPKα1 inhibition, cells were treated with Compound C (CC, 5 μM, Sigma-Aldrich, St Louis, G13418) for 6 h. For amino acid starvation, cells were treated with Grey's Balanced Salt Solution (GBSS; Sigma-Aldrich, G9779) for 1–3 h. Autophagic vacuoles were measured using an autophagy detection kit (Abcam, ab139484).

Oil red staining

After fixation with 2 ml fixative solution per well for 30 min, the prepared oil red O working solution (Beyotime, China, C0158M) was stained at room temperature for 10–20 min, and the liver cells washed twice with the washing solution were observed under a microscope (Mitsubishi Inc., Japan, S154).

Immunofluorescence

Immunofluorescence was performed using primary antibodies against *Tom20* (1: 200, Abcam, ab283317), *LAMP2* (1: 200, Abcam, ab199946), *Cyt-c* (1: 200, Abcam, ab216971), *P-AMPKα1* (1: 200, Wanleibio., China, WL02256) and *Parkin* (1: 500, Cell Signaling Technology, Inc, 4211). Cells were fixed in 4% paraformaldehyde and permeabilized (Biosharp, BL539A) with 0.1% TritonX-100, blocked with goat serum and incubated with primary antibodies, followed by appropriate secondary antibodies. The following secondary antibodies included Dylight 488-goat anti-rabbit lgG and Alexa Fluor 594-goat anti-mouse lgG. The nuclei were stained using DAPI (ImmunoBioscience, AR-6501–01). Images acquired by an Eclipse Ni-U microscope system (Nikon, N54) and a confocal laser scanning microscopy (Olympus, BX-61).

Oxidative stress biomarker assay

Liver tissues were homogenized in normal saline, and the supernatant collected for the following assays: total antioxidant capacity (T-AOC), glutathione peroxidase (GPX), superoxide dismutase (SOD), malondialdehyde (MDA) and catalase (CAT) (Beyotime, China, S0119 for T-AOC, S0058 for GSH-Px, S0087 for SOD, S0131M for MDA, S0082 for CAT), according to the manufacturer's protocols as previously described [32]. T-AOC could be used to evaluate the antioxidant capacity of biologically active substances. For MDA measurement, tissues were homogenized in MDA kit extract buffer and assayed according to the manufacturer's instructions [33].

Mitochondrial function analysis

Mitochondrial membrane potential ($\Delta\Psi$ m) was evaluated with mitochondrial membrane potential probe (JC-1) (Thermo, US, T3168) staining as described previously [34, 35]. Briefly, 3×10^5 cells were stained with 2 μL of JC-1 stock solution (final concentration: 2 μg/mL). Stained cells were observed by fluorescence microscopy at 500 nm (JC-1 monomers) 590 nm (JC-1 aggregates). Apoptosis was assessed with the YO-PRO-1 (green fluorescent) and PI (red fluorescent) apoptosis and necrosis detection kit (Beyotime, China, C2022-0.2 ml). The relative expression of the two dyes determines the level of apoptosis and necrosis. Mitochondrial ROS (mtROS) levels were detected by labeling 2×10^5 cells with the mitoSOX™ red mitochondrial superoxide indicator (Molecular Probes, USA, M36008), and analyzed by a flow cytometry.

RNA interference

For knockdown of SELENOM and *Parkin*, cells (3×10^5/well) were transfected with siRNA against SELENOM (A04066) or *Parkin* (A04091) using Lipofectamine (LIP) RNAi MAX Reagent according to the manufacturer's instruction. To overexpress SELENOM, a pcDNA3.1 vector containing the SECIS element was used according to the method of Gladyshev et al. [36]. The coding regions of mouse SELENOM were amplified by PCR and subcloned into the pcDNA3.1 vector to generate the pcDNA3.1-SELENOM plasmid, followed by verification by sequencing. Cells were transfected with plasmid pcDNA3.1-SELENOM using the LIP 2000 reagent (Invitrogen, USA, 11668030) in an Opti-MEM medium for 24 h.

RNA isolation and quantitative real-time polymerase chain reaction (qRT-PCR)

Total RNA was extracted from liver and AML12 hepatocytes following the manufacturer's protocol [37, 38]. cDNA was synthesized from 2 to 5 μg total RNA using a ReverTra Ace® qPCR RT Kit & Master Mix (Accurate Biotechnology Co., Ltd., SQ-101). qRT-PCR was performed using the Light Cycler®480 System (Roche, Beijing, China, 015278001) and ChamQ™ Universal SYBR® qPCR Master Mix (Vazyme

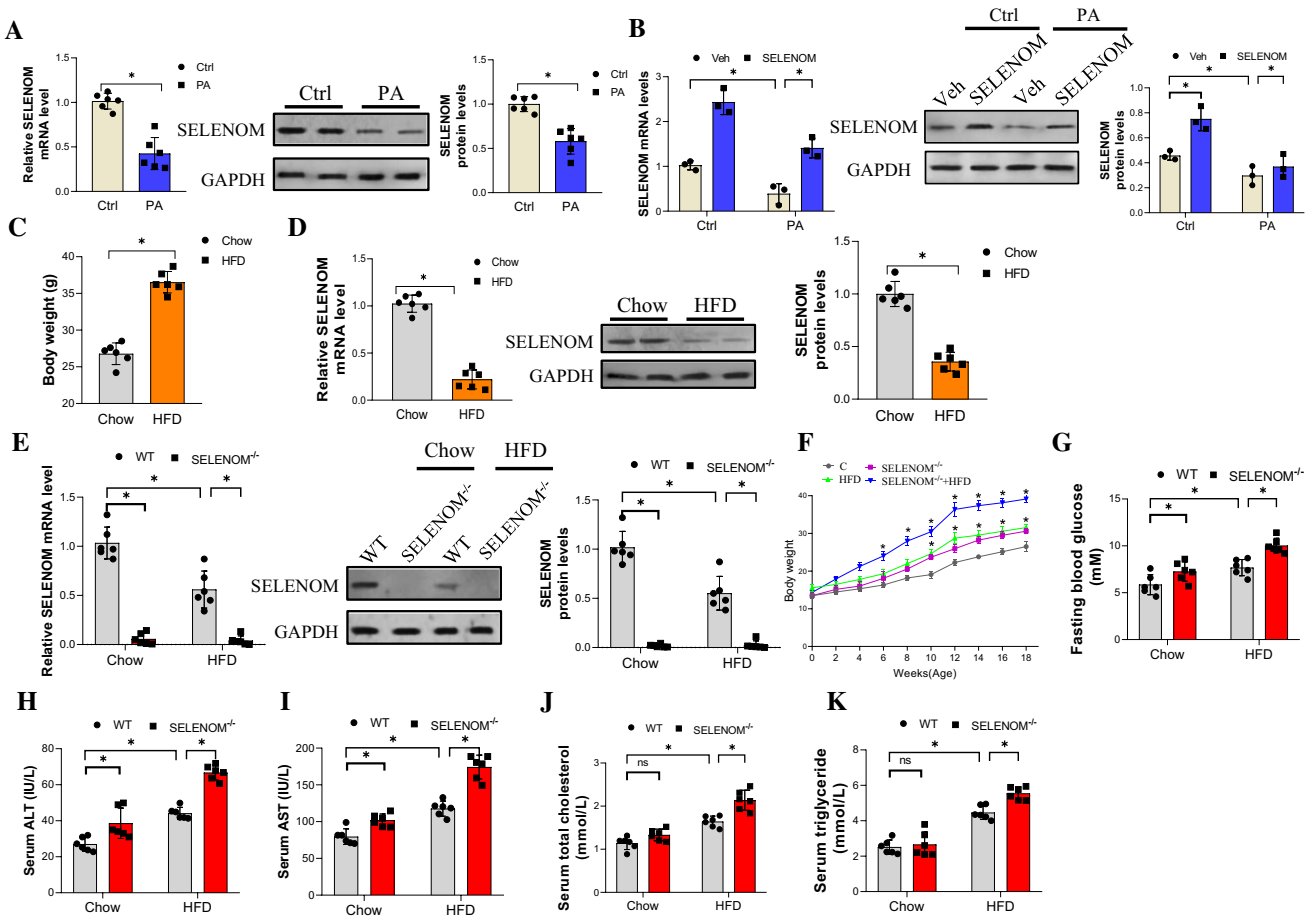

Fig. 1 SELENOM is downregulated in livers from HFD-treated mice and related to the development of NAFLD. **A** The mRNA and protein level of SELENOM in AML12 hepatocytes treated with PA (75 μM) ($n=6$; $^*P<0.05$). **B** The mRNA and protein level of SELENOM in vitro were detected in Veh, SELENOM, PA and SELENOM + PA ($n=3$; $^*P<0.05$). **C** Bodyweight of Chow- and HFD-treated mice ($n=6$; $^*P<0.05$). **D** The mRNA and protein level of SELENOM in livers from Chow- and HFD-treated mice (18 W) ($n=6$; $^*P<0.05$). **E** The mRNA and protein level of SELENOM was measured in livers from WT, SELENOM$^{-/-}$, HFD, SELENOM$^{-/-}$ + HFD ($n=6$; $^*P<0.05$). **F** Bodyweight in mice of WT, SELENOM$^{-/-}$, HFD and SELENOM$^{-/-}$ + HFD ($n=6$; $^*P<0.05$). **G–K** Blood glucose levels, ALT, AST, triglyceride, total cholesterol in the blood serum isolated from WT, SELENOM$^{-/-}$, HFD and SELENOM$^{-/-}$ + HFD mice ($n=6$; $^*P<0.05$). Values represent means ± SEM

Biotech Co., Ltd, Nanjing, China, azyme #Q711). The primers for target genes by qRT-PCR are shown in Table S2. GAPDH was used as an internal reference. The relative mRNA abundance was calculated by the $2^{-\Delta\Delta Ct}$ method [39].

Protein extraction and western blot analysis

Samples were lysed with RIPA lysis solution for total protein extraction, and quantification by BCA protein quantitative kit (Beyotime, China, P0012S). Proteins (30–40 μg per sample) were separated by SDS polyacrylamide gel electrophoresis and transferred to nitrocellulose membrane. Membranes were blocked with 5% bovine serum albumin (BSA) and incubated with primary antibodies (Table S3), followed by secondary antibodies. Stained proteins were visualized with enhanced chemiluminescent (ECL) substrate (Sigma-Aldrich, Germany, GE3541), imaged and normalized to GAPDH expression.

Quantification and statistical analysis

The GraphPad Prism 9.0 software (Graph Pad Software Inc., San Diego, CA, USA) was used for statistical analysis. Analyzed data are presented as mean ± SEM of triplicate samples ($n=3$) for in vitro experiments, and six replicates ($n=6$) for in vivo experiments. Statistical analyses were performed one-way ANOVA with Tukey's post hoc test. All data in this study followed normal distribution. Significance level was set at $^*P<0.05$. Representative images were quantified by Image-Pro Plus 6.0 software (Media cybernetics Image

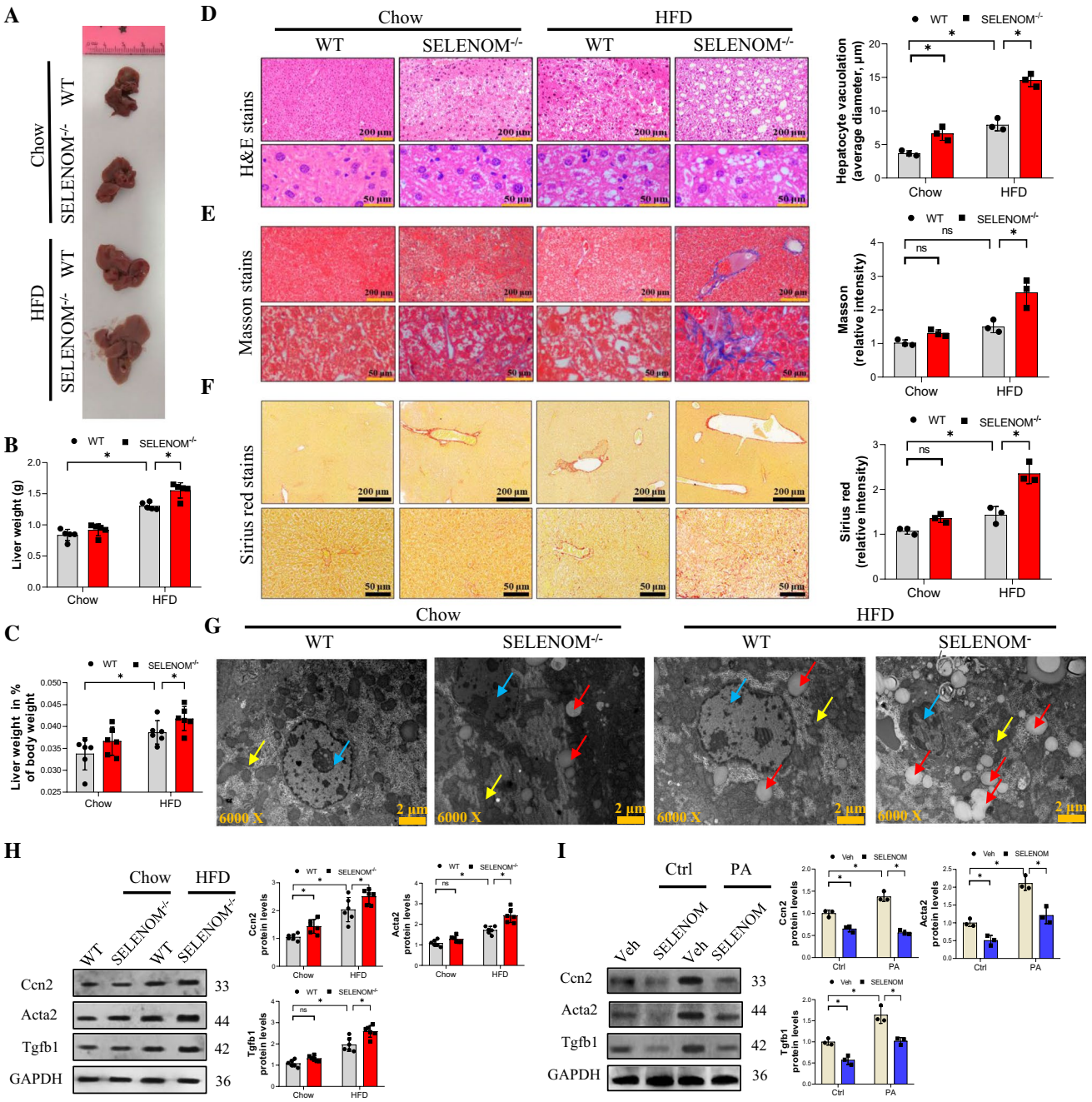

Fig. 2 Mice lacking SELENOM are more susceptible to NAFLD under HFD treatment. **A**, **B** The liver weight was measured in HFD-treated livers with SELENOM$^{-/-}$ ($n=6$; $^{*}P<0.05$). **C** The liver weight in % of body weight in HFD-treated livers with SELENOM-KO ($n=6$; $^{*}P<0.05$). **D** H&E staining shows steatosis in HFD-treated livers with SELENOM$^{-/-}$ (scale bar, 200 and 50 μm). Fields from one representative experiment of three are shown ($n=3$; $^{*}P<0.05$). **E**, **F** Masson and Sirius Red staining show bridging fibrosis (scale bar, 200 and 50 μm). Fields from one representative experiment of three are shown ($n=3$; $^{*}P<0.05$). **G** TEM images for liver from WT, SELENOM$^{-/-}$, HFD and SELENOM$^{-/-}$ + HFD. The blue arrow indicates the nucleus, the yellow arrow indicates the mitochondria and the red arrow indicates the accumulated lipid droplets. Scale bars, 2 μm. Images were chosen from three independent biological samples ($n=6$). **H** The protein levels of *Ccn2*, *Acta2* and *Tgfb1* were measured in WT, SELENOM$^{-/-}$, HFD and SELENOM$^{-/-}$ + HFD ($n=6$; $^{*}P<0.05$). **I** Liver fibrosis-related proteins in vitro were detected in Veh, SELENOM, PA and SELENOM + PA ($n=3$; $^{*}P<0.05$). Values represent means ± SEM

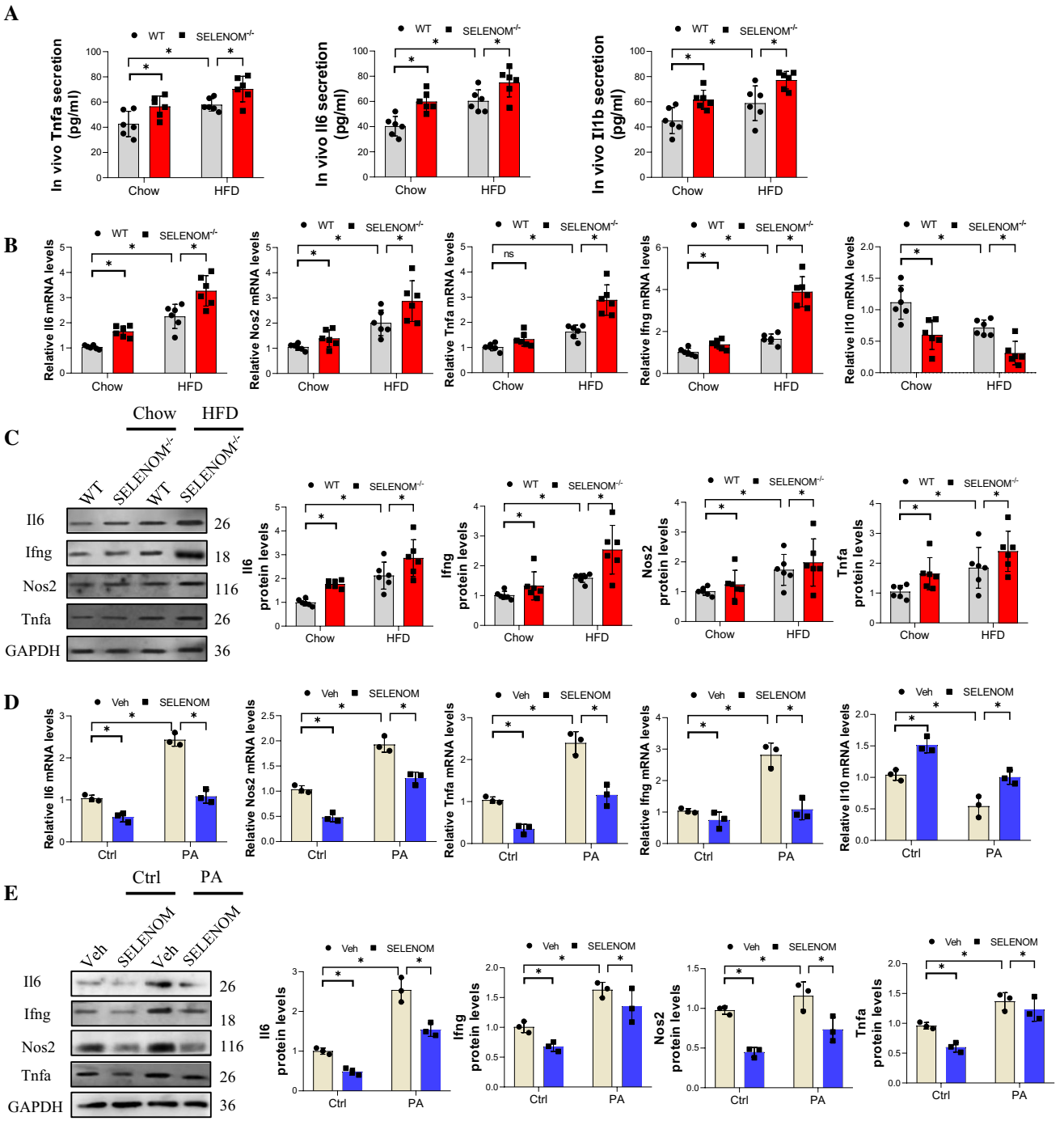

Fig. 3 SELENOM$^{-/-}$ increases HFD-mediated inflammation response in liver tissues. **A** The contents of cytokines (*Tnfa*, *Il6* and *Il1b*) in blood serum ($n=6$; $^*P<0.05$). **B**, **C** The mRNA and protein levels of inflammation response-related genes such as *Il6*, *Il10*, *Nos2* and *Tnfa* were determined by qRT-PCR (**B**) and WB (**C**) in HFD-treated livers with SELENOM$^{-/-}$ ($n=6$; $^*P<0.05$). **D**, **E** The mRNA and protein levels of inflammation response-related genes such as *Il6, Il10, Nos2* and *Tnfa* were detected in Veh, SELENOM, PA and SELENOM + PA ($n=3$; $^*P<0.05$). Values represent means ± SEM

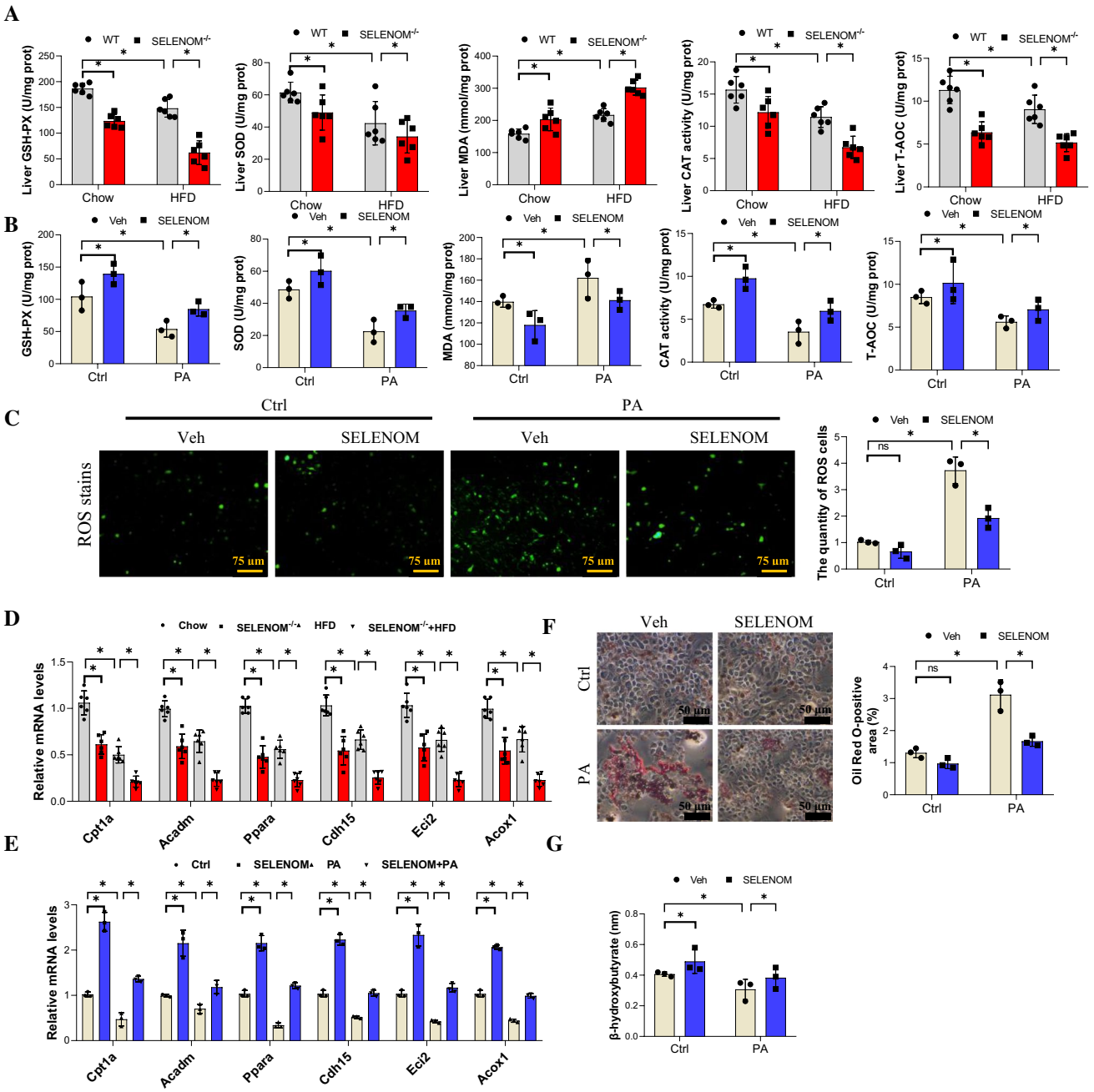

Fig. 4 SELENOM$^{-/-}$ increases HFD-induced hepatic oxidative stress. **A** Oxidative stress markers of the GSH-PX, SOD, MDA, CAT, T-AOC contents were measured in the livers from WT, SELENOM$^{-/-}$, HFD and SELENOM$^{-/-}$ + HFD ($n = 6$; $^*P < 0.05$). **B** Oxidative stress markers of the GSH-PX, SOD, MDA, CAT, T-AOC contents were measured in hepatocytes of Veh, SELENOM, PA and SELENOM + PA ($n = 3$; $^*P < 0.05$). Fields from one representative experiment of three are shown. **C** ROS staining was detected by immunofluorescence with DCFH-DA (green fluorescence, 5 mM) in hepatocytes of Veh, SELENOM, PA and SELENOM + PA ($n = 3$; $^*P < 0.05$). **D** The mRNA levels of lipogenic genes such as *Cpt1a*, *Acadm*, *Ppara*, *Cdh15*, *Eci2* and *Acox1* in HFD-treated livers with SELENOM$^{-/-}$ ($n = 6$; $^*P < 0.05$). **E** The mRNA levels of lipogenic genes such as *Cpt1a*, *Acadm*, *Ppara*, *Cdh15*, *Eci2* and *Acox1* in Veh, SELENOM, PA and SELENOM + PA ($n = 3$; $^*P < 0.05$). **F** Oil Red O staining in hepatocytes of Veh, SELENOM, PA and SELENOM + PA. Ten fields (Scale bar: 50 μm) were randomly selected for each sample. The positive area in each image was measured ($n = 3$; $^*P < 0.05$). **G** β-hydroxybutyrate contents were measured in the livers from WT, SELENOM$^{-/-}$, HFD and SELENOM$^{-/-}$ + HFD ($n = 6$; $^*P < 0.05$). Values represent means ± SEM

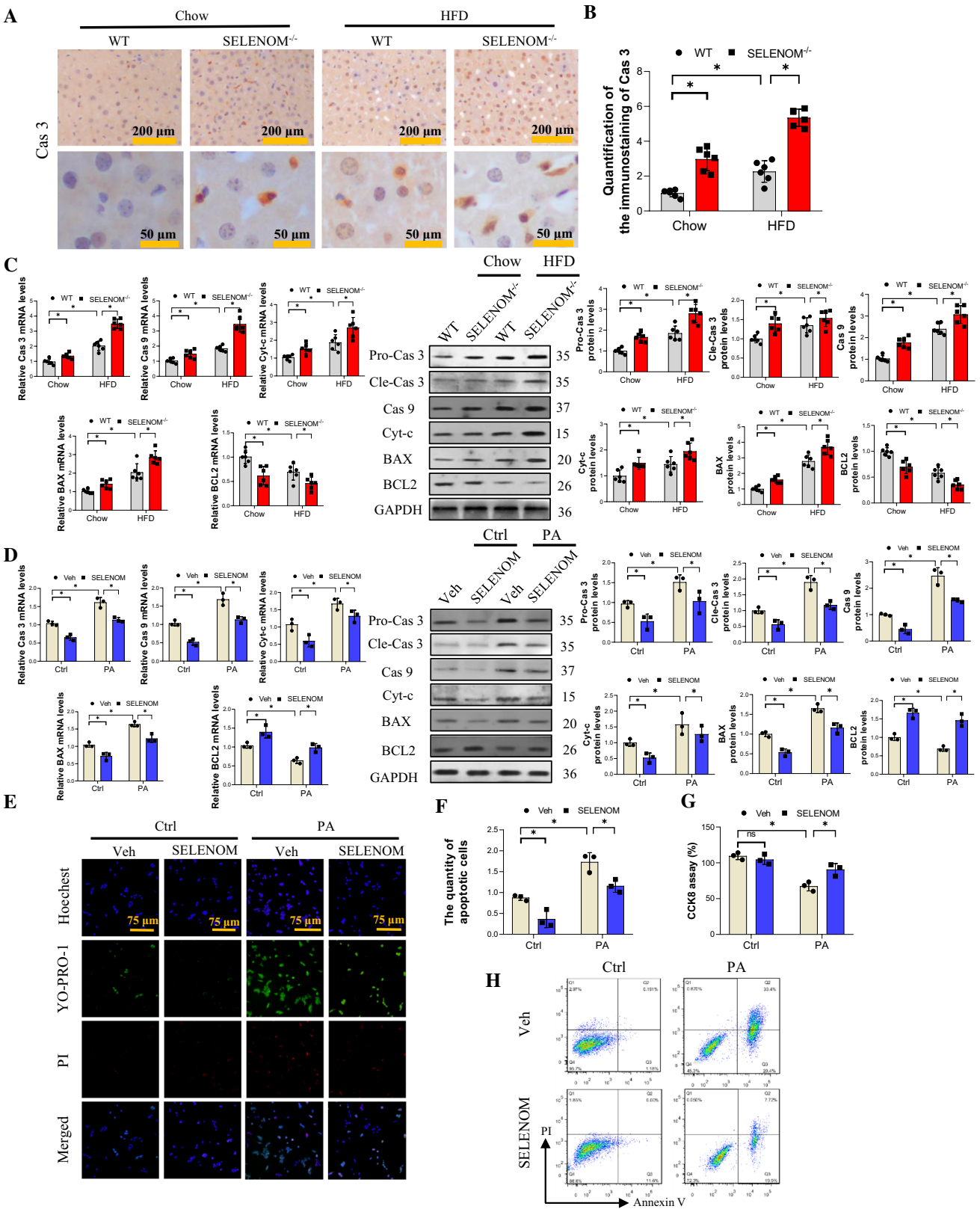

Technology Co., Ltd, USA) and statistically analyzed by the GraphPad Prism 9.0 software.

Results

◂**Fig. 5** SELENOM$^{-/-}$ increases HFD-mediated mitochondrial pathway apoptosis in the liver. **A**, **B** *Cas 3* was measured via immunohistochemistry analysis in livers from WT, SELENOM$^{-/-}$, HFD and SELENOM$^{-/-}$ + HFD. Six fields (Scale bar: 200 and 50 μm) were randomly selected for each sample. The positive area in each image was measured ($n = 6$; $^*P < 0.05$). **C** The mRNA and protein expression levels of mitochondrial pathway apoptosis-related genes *Cas 3*, *Cas 9*, *Bax* and *Bcl2* were determined in HFD-treated livers with SELENOM$^{-/-}$ ($n = 6$; $^*P < 0.05$). **D** The mRNA and protein expression levels of mitochondrial pathway apoptosis-related genes *Cas 3*, *Cas 9*, *Bax* and *Bcl2* were determined in hepatocytes of Veh, SELENOM, PA and SELENOM + PA ($n = 3$; $^*P < 0.05$). **E**, **F** Apoptosis and necrosis staining with YO-PRO-1 and PI for apoptosis detection, and the green nucleus represent an apoptotic cell ($n = 3$; $^*P < 0.05$). Fields from one representative experiment of three are shown. **G** CCK8 assay was used to assess the hepatocyte viability under PA treatment ($n = 3$; $^*P < 0.05$). **H** Cell viabilities and apoptosis rates were determined by flow cytometry. Healthy (Q1), early apoptotic (Q2), late apoptotic (Q3), and necrotic populations (Q4). Images were chosen from three independent biological samples ($n = 3$; $^*P < 0.05$). Values represent means ± SEM

SELENOM deletion aggravates HFD-induced NAFLD

To verify whether SELENOM is involved in NAFLD, an in vitro model of palmitic acid (PA)-mediated lipotoxicity and a mouse model of HFD-induced NAFLD were established, and the level of SELENOM detected with qRT-PCR and western blot. In culture, SELENOM level was significantly reduced in PA-treated hepatocytes at both the mRNA and protein expression levels, compared to the untreated control cells (Fig. 1A). This reduction in SELENOM level by PA treatment can be reversed by overexpression of SELENOM (Fig. 1B). In vivo, mice fed with HFD for 18 weeks showed significantly higher weight (Fig. 1C), and increases in hepatic lipid metabolism parameters including alanine transaminase (ALT), aspartate transaminase (AST), total cholesterol and triglycerides (see Fig. 1H–K wild-type mice data). The liver of these mice showed lower mRNA and protein levels of SELENOM compared to normal chow-fed mice (Fig. 1D). This suggests that HFD downregulates SELENOM expression in the liver. To dive deeper into the role of SELENOM in NAFLD, we generated SELENOM knockout (SELENOM$^{-/-}$) mice (Fig. S1A) with no expression of SELENOM in the liver (Fig. 1E). Immunohistochemistry result revealed that SELENOM expression was markedly lowered in the cytoplasm of hepatocytes of HFD-fed and SELENOM$^{-/-}$ mice compared with the chow group (Fig. S1B–C). Data related to the mRNA expression of SELENOM in other tissues are shown (Fig. S1D). Comparing the biological characteristics (bodyweight, blood glucose and metabolic parameters) of HFD-fed and SELENOM$^{-/-}$ mice showed that bodyweight (Fig. 1F) and blood glucose content (Fig. 1G) were increased in mice fed with HFD, and were even higher in SELENOM$^{-/-}$ mice. Similarly, the high levels of ALT, AST, total cholesterol and triglycerides in the serum of HFD-fed mice were further aggravated by SELENOM knockdown (Fig. 1H–K). Altogether, these data suggested that HFD downregulates SELENOM, and SELENOM deletion aggravates the development of HFD-induced fatty liver disease.

SELENOM deletion induces hepatic injury in HFD treatment

Analysis of the gross liver morphology showed that the liver of HFD-fed mice was significantly larger and heavier than those of chow-fed mice, and SELENOM$^{-/-}$ mice showed further increase in liver weight when fed HFD (Fig. 2A, B). The liver weight in % of body weight was consistent with the trend of body weight (Fig. 2C). H&E staining showed that HFD increased hepatic vacuolization and steatosis, which were further enhanced in the liver of SELENOM$^{-/-}$ mice, particularly with they were fed with HFD (Fig. 2D). Similarly, the increased liver fibrosis caused by HFD, shown by Masson and Sirius Red staining, was also further exacerbated in SELENOM$^{-/-}$ mice (Fig. 2E, F). These increases in steatosis, nuclear atrophy and overall liver degeneration were further validated by transmission electron microscopy (Fig. 2G). At the molecular level, many liver fibrosis-related genes including *Cox I*, *Cox IV*, *Ccn2*, *Acta2*, *Tgfb1*, *Timp1*, *Ccn1*, *Ccn2*, *Vim* and *Mmp9* were significantly increased by HFD, and further increased by SELENOM deletion (Fig. S2A). The protein expressions of *Ccn2*, *Tgfb* and *Acta2* were also similarly increased in vitro (Fig. 2H). These in vivo changes in liver fibrosis-related genes and proteins were recapitulated in PA-induced lipotoxicity cultures, and reversed by SELENOM overexpression in hepatocytes (Figs. 2I and S2B). Together, these results suggest that SELENOM deletion increases HFD-mediated hepatic alveolar steatosis and fibrosis.

SELENOM deletion increases inflammation response in HFD-induced liver.

Chronic inflammation is a critical histological change in NAFLD [40, 41], contributing to fibrosis, cirrhosis, liver failure and even hepatocellular carcinoma. Thus, we evaluated the effect of HFD and SELENOM deletion on liver inflammation, and found that both conditions significantly increased the serum levels of *Tnfa*, *Il6*, and *Il1b* compared to the chow-fed group; SELENOM$^{-/-}$ mice fed with HFD showed even higher levels of these proteins (Fig. 3A). In the

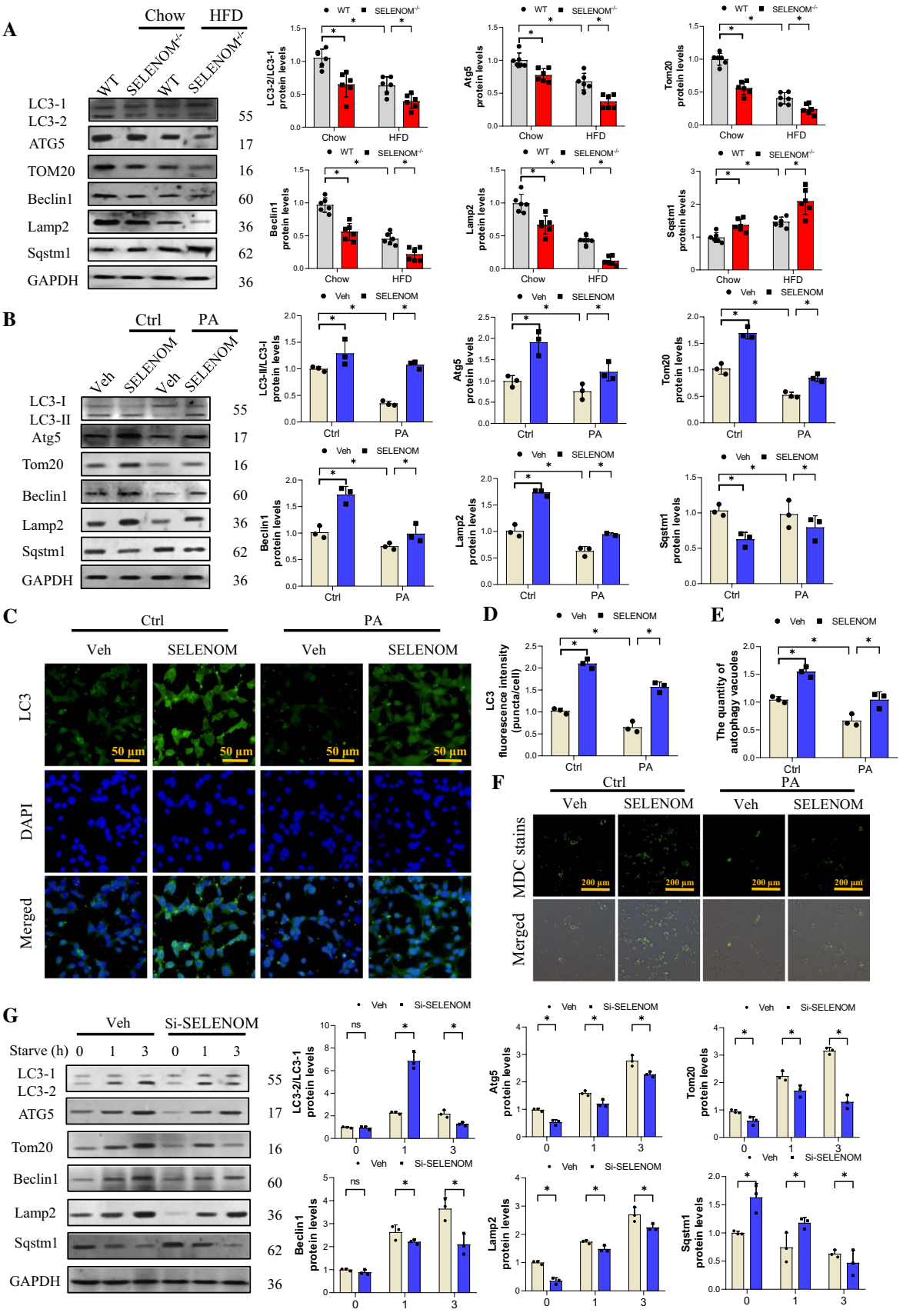
A
Chow
HFD
WT
SELENOM-/-
WT
SELENOM-/-
LC3-1
LC3-2
ATG5
TOM20
Beclin1
Lamp2
Sqstm1
GAPDH
55
17
16
60
36
62
36
LC3-2/LC3-1 protein levels
Atg5 protein levels
Tom20 protein levels
Beclin1 protein levels
Lamp2 protein levels
Sqstm1 protein levels
B
Ctrl
PA
Veh
SELENOM
LC3-I
LC3-II
Atg5
Tom20
Beclin1
Lamp2
Sqstm1
GAPDH
55
17
16
60
36
62
36
LC3-II/LC3-I protein levels
C
LC3
DAPI
Merged
50 μm
D
LC3 fluorescence intensity (puncta/cell)
E
The quantity of autophagy vacuoles
F
MDC stains
Merged
200 μm
G
Si-SELENOM
Starve (h)
0
1
3
ns

◂**Fig. 6** SELENOM involves in HFD-inhibited mitophagy in the liver. **A** The expression levels of mitophagy-related proteins such as *LC3-I*, *LC3-II*, *Atg5*, *Tom20*, *Beclin1*, *Lamp2* and *Sqstm1* in livers from WT, SELENOM$^{-/-}$, HFD and SELENOM$^{-/-}$ + HFD ($n=6$; $^{*}P<0.05$). **B** The expression levels of mitophagy-related proteins such as *LC3-I*, *LC3-II*, *Atg5*, *Tom20*, *Beclin1*, *Lamp2* and *Sqstm1* in hepatocytes of Veh, SELENOM, PA and SELENOM + PA ($n=3$; $^{*}P<0.05$). **C**, **D** Immunofluorescence assay for mitophagy via assessing *LC3* in vitro. Fields from one representative experiment of three are shown ($n=3$; $^{*}P<0.05$). **E**, **F** The quantity of autophagy vacuoles was recorded by MDC staining. Fields from one representative experiment of three are shown ($n=3$; $^{*}P<0.05$). **G** Immunoblotting for *LC3-I*, *LC3-II*, *Atg5*, *Tom20*, *Beclin1*, *Lamp2* and *Sqstm1* in AML12 hepatocytes treated with Si-NC or Si-SELENOM were subjected to amino acid starvation for the indicated durations, 0, 1, 3 h, respectively ($n=3$; $^{*}P<0.05$). Values represent means ± SEM

liver, the gene and protein levels of the pro-inflammatory cytokines *Il6*, *Ifng*, *Nos2* and *Tnfa* were similarly increased by HFD and SELENOM deletion (Fig. 3B, C). On the other hand, the mRNA level of the anti-inflammatory factor Il10 was decreased by HFD and SELENOM deletion (Fig. 3B). Again, these observations could be reproduced in vitro with PA treatment, which increased the mRNA and protein levels of *Il6*, *Ifng*, *Nos2* and *Tnfa*, and decreased *Il10*; SELENOM overexpression counteracted these effects (Fig. 3D, E). Taken together, these results support that SELENOM deletion may exacerbate HFD-induced hepatic inflammation.

SELENOM$^{-/-}$ increases HFD-mediated oxidative stress and attenuates fatty acid oxidation (FAO) in liver tissues

Recent evidence has shown that oxidative stress and FAO play an important role in hepatocyte lipid metabolism and the pathogenesis of NAFLD [42]. Thus, we evaluated these pathways in liver samples and found that HFD reduced the level of CAT, GPX, SOD and T-AOC, and SELENOM deletion further reduced these antioxidant enzymes when combined with HFD (Fig. 4A). By comparison, the lipid peroxidation marker malondialdehyde (MDA) was elevated by HFD, and further enhanced in SELENOM$^{-/-}$ mice fed with HFD. In vitro results show that PA treatment could reduce the levels of CAT, SOD, GPX and T-AOC, and increase the level of MDA; all changes were reversed by SELENOM overexpression (Fig. 4B). In addition, ROS were significantly increased in PA-treated hepatocytes, and this was reduced in hepatocytes with SELENOM overexpression (Fig. 4C). Together, these data indicate that SELENOM deletion increases oxidative stress in the presence of HFD.

For the lipid metabolism pathway, we found that the FAO-related genes *Cpt1a*, *Acadm*, *Ppara*, *Cdh15*, *Eci2* and *Acox1* were downregulated in HFD-fed mice, and further decreases were seen in SELENOM$^{-/-}$ mice on HFD (Fig. 4D). In vitro results show that PA treatment also decreased the expression of these genes in hepatocytes, and the effect was reversed by SELENOM overexpression (Fig. 4E). Conversely, the levels of lipogenic genes *Gpam*, *Plin1*, *Scd1*, *Lipe*, *Fasn*, *Acly* and *Pparg* were increased by HFD and further enhanced in SELENOM$^{-/-}$ mice on HFD (Fig. S3A). As expected, SELENOM overexpression could inhibit PA induction of these lipogenic genes (Fig. S3B). In addition, siRNA knockdown of SELENOM enhanced the mRNA level of these lipogenic genes and aggravated PA-induced lipid accumulation (Fig. S3C). Oil red staining showed that SELENOM overexpression could inhibit PA-induced lipid accumulation, and restore the level of beta-hydroxybutyrate, a metabolic product of beta-oxidation (Fig. 4F, G). Together, these data underscore the effects of SELENOM deficiency in decreasing FAO and increasing lipid deposition in HFD-fed mice.

SELENOM attenuates hepatocyte mitochondrial pathway apoptosis

The mitochondrial apoptosis pathway plays an important role in the lipotoxicity of the hepatocyte [43, 44]. Accordingly, we observed that *caspase 3* (*Cas3*) staining was increased in the liver of HFD-treated mice, and further enhanced by SELENOM deletion (Fig. 5A, B). This result was supported with observations of increased mitochondrial pro-apoptotic genes and proteins including *Bax*, Cyt-c, pro- and cleaved-*Cas3* and *Cas 9*, in HFD-fed mice, an effect that was strengthened by SELENOM deletion (Fig. 5C). In contrast, the level of the anti-apoptotic factor Bcl2 was downregulated. These results were reproducible in vitro with PA-induced hepatocyte apoptosis where the suppression of *Bax*, Cyt-c, *Cas3* and *Cas9* expressions, and enhancement of *Bcl2* was reversed by SELENOM overexpression (Fig. 5D). Consistent with this, results of YO-PRO-1/PI apoptosis staining, CCK8 cell viability assay and annexin V staining all demonstrate that PA treatment enhanced apoptosis, which was reversed by SELENOM overexpression (Fig. 5E–H). Taken together, these data illustrate that SELENOM deletion augments mitochondrial apoptosis induced by HFD and this can be attenuated by SELENOM overexpression.

SELENOM$^{-/-}$ attenuates hepatocyte mitophagy activity

Mitophagy maintains mitochondria quality by removing damaged mitochondria with the help of lysosomes [45]. We evaluated mitophagy-related factors and found that HFD diminished the ratio of *LC3-II/LC3-I*, and the levels of *Beclin1* and *Atg5*; HFD-fed SELENOM$^{-/-}$ mice exhibited even

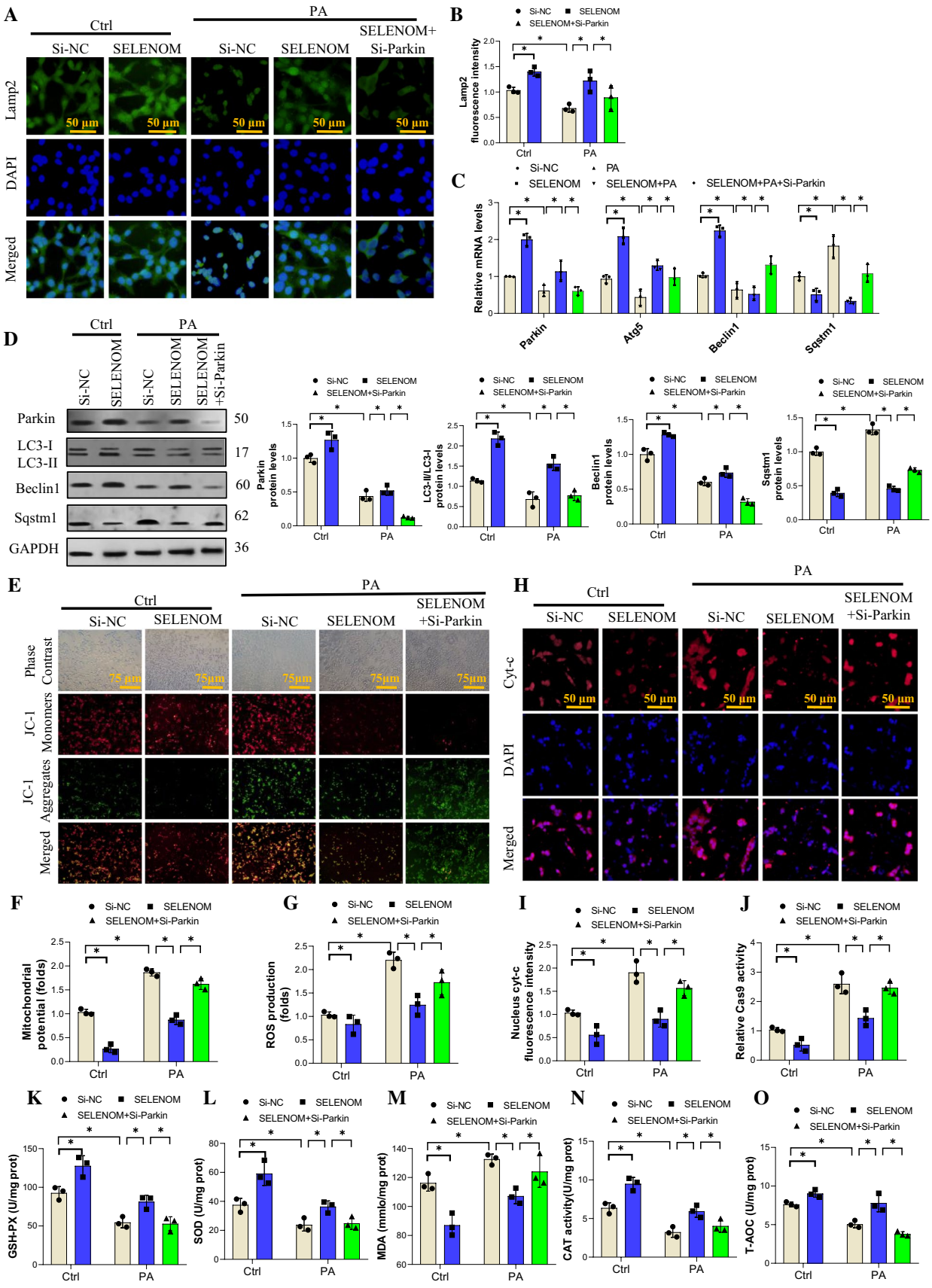
A
Ctrl
PA
Si-NC
SELENOM
Si-NC
SELENOM
SELENOM+ Si-Parkin
Lamp2
DAPI
Merged
50 μm
B
Si-NC
SELENOM
SELENOM+Si-Parkin
Lamp2 fluorescence intensity
Ctrl
PA
C
Si-NC
PA
SELENOM
SELENOM+PA
SELENOM+PA+Si-Parkin
Relative mRNA levels
Parkin
Atg5
Beclin1
Sqstm1
D
Ctrl
PA
Si-NC
SELENOM
Si-NC
SELENOM
SELENOM +Si-Parkin
Parkin
LC3-I
LC3-II
Beclin1
Sqstm1
GAPDH
50
17
60
62
36
Parkin protein levels
LC3-II/LC3-I protein levels
Beclin1 protein levels
Sqstm1 protein levels
E
Ctrl
PA
Si-NC
SELENOM
Si-NC
SELENOM
SELENOM +Si-Parkin
Phase Contrast
JC-1 Monomers
JC-1 Aggregates
Merged
75 μm
H
Ctrl
PA
Si-NC
SELENOM
Si-NC
SELENOM
SELENOM +Si-Parkin
Cyt-c
DAPI
Merged
50 μm
F
Mitochondrial potential (folds)
G
ROS production (folds)
I
Nucleus cyt-c fluorescence intensity
J
Relative Cas9 activity
K
GSH-PX (U/mg prot)
L
SOD (U/mg prot)
M
MDA (mmlo/mg prot)
N
CAT activity(U/mg prot)
O
T-AOC (U/mg prot)

◂**Fig. 7** SELENOM regulates in PA-inhibited mitophagy by activating *Parkin*. **A**, **B** The immunofluorescent intensity of *Lamp2* was verified via immunofluorescence assay in groups of Si-NC, SELENOM, PA + Si-NC, SELENOM + PA and SELENOM + PA + Si-Parkin ($n = 3$; $^*P < 0.05$). Si-Parkin (50 nM) was used to block *Parkin* expression. Fields from one representative experiment of three are shown. **C**, **D** The mRNA and protein expression levels of mitophagy-related genes such as *Parkin*, *LC3*, *Beclin1* and *Sqstm1* were determined in hepatocytes of Si-NC, SELENOM, PA + Si-NC, SELENOM + PA and SELENOM + PA + Si-Parkin ($n = 3$; $^*P < 0.05$). **E**, **F** Mitochondrial membrane potential was detected by the JC-1 staining ($n = 3$; $^*P < 0.05$). Representative images were chosen from three independent biological samples (scale bar, 75 μm). **G** ROS production stained by DCFH-DA (5 mM) was measured by a fluorescence microplate reader. The data represent the mean ± SEM ($n = 3$; $^*P < 0.05$). **H**, **I** Immunofluorescent intensity of *Cyt-c* was verified via immunofluorescence assay ($n = 3$; $^*P < 0.05$). Fields from one representative experiment of three are shown (scale bar, 50 μm). **J** The mRNA of *Cas 9* was determined in hepatocytes of Si-NC, SELENOM, PA + Si-NC, SELENOM + PA and SELENOM + PA + Si-Parkin ($n = 3$; $^*P < 0.05$). **K–O** The contents of GSH-PX, SOD, MDA, CAT, T-AOC were measured in hepatocytes of Si-NC, SELENOM, PA + Si-NC, SELENOM + PA and SELENOM + PA + Si-Parkin ($n = 3$ per group, $^*P < 0.05$ versus the difference between groups). The data represent the mean ± SEM

further reduction (Fig. 6A). Moreover, the protein level of Sqstm1 was elevated in HFD-fed mice and further increased in HFD-fed SELENOM$^{-/-}$ mice. The mitochondrial protein *Tom20* and lysosomal protein *Lamp2* were downregulated in HFD-fed mice, but the decreases were much greater in SELENOM$^{-/-}$ mice on HFD, indicating that mitophagy was impaired in SELENOM$^{-/-}$ mice under high-fat stress. As expected, mRNA expression levels of these mitophagy-related genes were consistent with the protein expression level (Fig. S4A). Consistent with the in vivo data, PA treatment also decreased the ratio of *LC3-II/LC3-I*, the levels of *Atg5*, *Tom20*, *Beclin1* and *Lamp2*, and increased the level of *Sqstm1*; SELENOM overexpression reversed the effect (Fig. 6B). The mRNA levels of these mitophagy-related genes were consistent with the protein expression levels (Fig. S4B). Immunofluorescence staining of *LC3* was consistent with the western blot data (Fig. 6C, D). Furthermore, we stained autophagy vacuoles with MDC and found that PA treatment reduced the number of vacuoles, and SELENOM overexpression reversed this effect (Fig. 6E, F), indicating that SELENOM may increase the number of autophagy vacuoles.

The autophagy activation model was established with amino acid starvation (AAS) [46] to further determine the role of SELENOM in mitophagy. As shown in Fig. 6G, AAS increased the ratio of *LC3-II/LC3-I*, levels of *Atg5*, *Tom20*, *Beclin1*, *Lamp2*, and reduced *Sqstm1* expression in a time dependent manner. SELENOM knockdown could decrease the levels of mitophagy induced by AAS of 1 or 3 h (Si-SELENOM; see Fig. S4C, D for the mRNA and protein levels of SELENOM after siRNA treatment). The mRNA levels of mitophagy-related genes were consistent with the protein levels (Fig. S4E). Together, these data indicate that SELENOM may regulate HFD-induced NAFLD via mitophagy pathways.

SELENOM modulates mitochondrial stress via activating the *Parkin*-related mitophagy

Parkin was found to be a major factor in mitophagy activation [47]. To determine whether *Parkin* contributes to SELENOM-modulated mitophagy, we first knockdown *Parkin* (Si-Parkin) in hepatocytes with siRNA and found that SELENOM level did not change (Fig. S5A). Immunofluorescence staining showed that *Lamp2* was reduced by PA stress and rescued by SELENOM overexpression; Si-Parkin abolished the effect of SELENOM (Fig. 7A, B). Evaluation of other mitophagy factors showed that PA treatment decreased the mRNA and protein expressions of *Parkin*, *LC3*, and *Beclin1*, and increased the expression of *Sqstm1*; SELENOM overexpression reversed these effects, and Si-Parkin blocked the action of SELENOM (Fig. 7C, D). We have shown above that PA treatment reduced the number of autophagy vacuoles and the effect was reversed by SELENOM overexpression; Addition of Si-Parkin also counteracted the effect of SELENOM in this setting (Fig. S5B, C). These results show that SELENOM activates mitophagy via enhancement of *Parkin* expression in response to PA-induced stress.

To further clarify the function of SELENOM in mitochondrial homeostasis, mitochondrial transmembrane potential was assessed by JC-1 staining in vitro. We found that the increased membrane potential induced by PA treatment could be ameliorated by SELENOM overexpression; however, this effect was abrogated by Si-Parkin treatment (Fig. 7E, F). Similarly, we observed that PA-induced up-regulation of mitochondrial ROS was attenuated by SELENOM overexpression in a *Parkin*-dependent manner as Si-Parkin treatment inhibited the effect of SELENOM (Fig. 7G).

The release of cytochrome C (*Cyt-c*) from the mitochondrial membrane into the nucleus/cytoplasm is a central step in the mitochondrial apoptosis pathway. Immunofluorescent staining shows that PA treatment increased *Cyt-c* release, while SELENOM overexpression mitigated this effect; *Parkin* siRNA transfection again inhabited the action of SELENOM (Fig. 7H, I). Levels of the apoptotic protein *Cas 9* were similarly induced by PA treatment, which was reversed by SELENOM overexpression in a *Parkin*-dependent manner (Fig. 7J). Moreover, the antioxidants GPX, SOD, CAT and T-AOC were all reduced by PA treatment, an effect that was inhibited by SELENOM overexpression, and *Parkin* deletion blocked the effect of SELENOM; for MDA the reverse is true since PA increased this factor, SELENOM overexpression reduced it, and Si-Parkin treatment abolished the effect of SELENOM (Fig. 7K–O). Altogether, our data

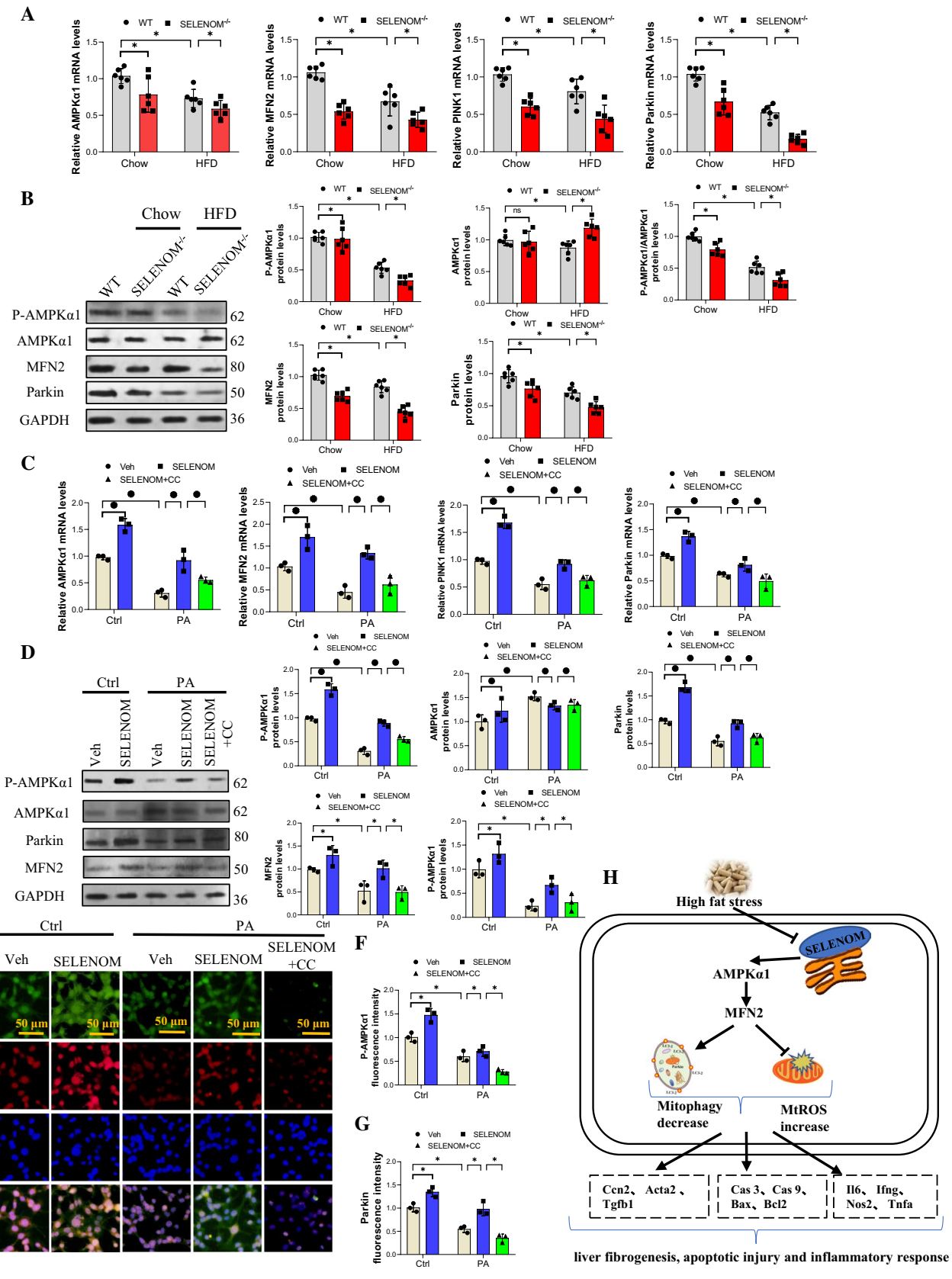
A
WT
SELENOM-/-
Relative AMPKα1 mRNA levels
Relative MFN2 mRNA levels
Relative PINK1 mRNA levels
Relative Parkin mRNA levels
Chow
HFD
B
Chow
HFD
WT
SELENOM-/-
P-AMPKα1
AMPKα1
MFN2
Parkin
GAPDH
62
62
80
50
36
P-AMPKα1 protein levels
AMPKα1 protein levels
P-AMPKα1/AMPKα1 protein levels
MFN2 protein levels
Parkin protein levels
ns
C
Veh
SELENOM
SELENOM+CC
Ctrl
PA
D
E
F
G
Ctrl
PA
Veh
SELENOM
SELENOM +CC
P-AMPKα1
Parkin
DAPI
Merged
50 μm
P-AMPKα1 fluorescence intensity
Parkin fluorescence intensity
H
High fat stress
SELENOM
AMPKα1
MFN2
Mitophagy decrease
MtROS increase
Ccn2、Acta2、Tgfb1
Cas 3、Cas 9、Bax、Bcl2
Il6、Ifng、Nos2、Tnfa
liver fibrogenesis, apoptotic injury and inflammatory response

◂**Fig. 8** SELENOM regulates *Parkin* via the *AMPKα1–MFN2* pathway. **A**, **B** The mRNA and protein expression levels of *AMPKα1*, *MFN2* and *Parkin* were determined in HFD-treated livers with SELENOM$^{-/-}$ ($n=6$; $^{*}P<0.05$). **C**, **D** The mRNA and protein levels of *AMPKα1*, *MFN2* and *Parkin* were determined in hepatocytes of Veh, SELENOM, PA, SELENOM + PA and SELENOM + PA + CC. Compound C (CC) was an inhibitor of *AMPKα1* to block the activation of *AMPKα1* ($n=3$; $^{*}P<0.05$). **E–G** The immunofluorescent intensity of *P-AMPKα1* and *Parkin* was verified via using the immunofluorescence assay in hepatocytes of Veh, SELENOM, PA, SELENOM + PA and SELENOM + PA + CC ($n=3$; $^{*}P<0.05$). Fields from one representative experiment of three are shown (scale bar, 50 μm). Values represent means ± SEM. **H** Schematic representation of SELENOM promoting *AMPKα1–MFN2* pathway in mitophagy of liver

indicate that under high-fat pressure, the protective effect of SELENOM overexpression on liver mitochondrial homeostasis and oxidative stress requires *Parkin*-related mitochondrial autophagy.

SELENOM regulates *Parkin* via the AMPKα1–MFN2 pathway

It has been reported that the *AMPKα1–MFN2* signaling pathway is involved in mitophagy [27, 28]. We evaluated this pathway in the liver of HFD-fed and SELENOM$^{-/-}$ mice and found that the mRNA levels of *AMPKα1*, *MFN2*, *PINK1* and *Parkin* were decreased by HFD and SELENOM deletion alone, but was further decreased in SELENOM$^{-/-}$ mice fed with HFD (Fig. 8A). Similarly, the protein levels of *MFN2* and *Parkin*, and the ratio of *P-AMPKα1/AMPKα1* were decreased in HFD-fed and SELENOM$^{-/-}$ mice, and further depleted in SELENOM$^{-/-}$ mice fed with HFD (Fig. 8B). These observations were reproducible in in vitro where PA stress decreased the mRNA and protein expressions of *AMPKα1*, *MFN2*, *PINK1* and *Parkin*, and the effects were nullified by SELENOM overexpression. Using an inhibitor of *AMPK*, Compound C (CC, 5 μM), we further showed that the effect of SELENOM can be abolished (Fig. 8C, D). These findings were also observable with *P-AMPKα1* and *Parkin* immunofluorescent staining (Fig. 8E–G). Together, these data suggest that SELENOM activates *Parkin* via the *AMPKα1–MFN2* pathway in hepatocytes.

Discussion

SELENOM has been shown to play a pivotal role in various liver diseases [3]. In this study, we show that SELENOM was downregulated in fatty liver disease and SELENOM deletion increased the susceptibility to fatty liver disease induced by HFD in mice. SELENOM deficiency aggravates HFD-mediated hepatic oxidative stress, mitochondria apoptosis, inflammation, steatosis, and fibrosis. Additionally, SELENOM regulates mitochondrial membrane potential and mitophagy, two routes through which mitochondrial apoptosis may be controlled. Mechanistically, we showed that SELENOM regulates *Parkin*-mediated mitophagy via the *AMPKα1–MFN2* signaling pathway; blockade of the *AMPKα1–MFN2* pathway could inhibit mitophagy and abolish the mitochondrial protective effects of SELENOM. Our findings, thus, reveal that manipulating SELENOM provides a potential opportunity for treating NAFLD (Fig. 8H).

Fibrosis is part of the pathological progression in NAFLD and is characterized by increased collagen deposition and inflammation. These features, including the activation of fibrosis markers *Ccn2*, *Tgfb* and *Acta2* and inflammatory cytokines *Tnfa*, *Il6*, *Ifng* and *Nos2*, were significantly increased in the absence of SELENOM. Steatosis is another pathological feature of NAFLD and reduction in FAO has been shown to increase lipid deposition and promote NAFLD development [48]. We showed that SELENOM deletion inhibits the expression of FAO-related genes (*Ppara*, *Cpt1α*, *Cdh15*, *Acox1* and *Acadm*), and increases the expression of lipogenic genes (*Gpam*, *Plin1*, *Scd1*, *Lipe*, *Fasn*, *Acly* and *Pparg*), thus contributes to lipid accumulation and steatosis. Based on these findings, our data suggest that SELENOM inhibition may be one of the reasons that aggravate fatty liver disease, hepatic steatosis, inflammation and liver fibrosis. Further studies are needed to examine the effects of SELENOM-mediated signal transduction on the pathogenesis of NAFLD.

SELENOM and thioredoxin have antioxidant activity and activate hypothalamic leptin signaling in the hypothalamus of mice [49]. SELENOM is mainly located in the brain, and overexpression of SelenoM in rats could improve Alzheimer's disease by inhibiting the activity of secretase in the brain [50]. Dietary selenium supplementation promotes the development of mature II oocytes in the ovaries of aging mice by increasing the expression of SELENOM [51]. SELENOM knockout mice gained weight and increased white adipose tissue levels, suggesting that SELENOM has a regulatory effect on energy homeostasis in the body [52]. Studies have shown that SELENOM can be expressed in primary murine neuronal cultures, HT-1080 (fibrosarcoma) and MCF-7 (breast adenocarcinoma), hepatocellular carcinoma, adipocytes, neutrophils and so on [53, 54]. SELENOM could prevent the increase in oxidative stress and mitochondria damage in Alzheimer's disease [7, 55], and reduces chondrocyte apoptosis by regulating oxidative stress and mitochondrial pathways [56]. Similarly, we show that SELENOM deletion in hepatocytes could induce excessive ROS production and unbalance the antioxidant system through decreasing the activity of SOD, GPX and T-AOC, resulting in mitochondrial metabolic dysfunction. Thus, SELENOM plays a key role in maintaining mitochondrial homeostasis in the

liver, SELENOM deletion could increase mitochondrial oxidative stress (mtROS) and mitochondrial potential disorder in hepatocytes. The loss of mitochondrial transmembrane potential could be related to the recruitment of the pro-mitophagy factor *Parkin* [57, 58]. In support of this concept, our results show that SELENOM overexpression could maintain mitochondrial transmembrane potential by activating *Parkin*-dependent mitophagy. SELENOM also diminishes apoptosis by protecting mitochondria function in chicken chondrocytes [7, 56]. Similarly, we show here that the loss of SELENOM was followed by activation of *Cas 3/Cas 9*-mediated apoptosis in hepatocytes. High-fat diet-induced liver apoptotic damage may be the root cause of lipid accumulation [59–61]. Accumulation of damaged mitochondria may be a major cause of oxidative stress damage in the liver, which can cause mitochondrial pathway apoptosis to liver cells. We also observed concomitant increase in liver apoptosis and lipid accumulation in SELENOM$^{-/-}$ mice. These data suggest that HFD-mediated hepatocyte injury is caused by mitochondrial dysfunction, and the downregulation of SELENOM may be a pathogenic factor in HFD-induced NAFLD.

Mitophagy defects are thought to induce NAFLD by allowing damaged mitochondria to accumulate [24]. Impaired mitophagy may contribute to the abnormal accumulation of lipid, but the underlying molecular mechanisms are unclear. Our data suggest that SELENOM is the upstream inhibitor of mitochondrial damage, as defective mitophagy was increased by HFD-stress and SELENOM deletion, and further exacerbated in SELENOM$^{-/-}$ mice fed with HFD. *Parkin* is one of the major activators of mitophagy. Lipid deposition in chronic alcoholic fatty liver is related to the *PINK1/Parkin* signaling pathway [25], and lipid accumulation induced by mitochondrial damage is associated with NAFLD in mice [62]. Based on these findings, we confirmed that SELENOM deletion may induce the accumulation of damaged mitochondria in NAFLD due to reduced activation of *Parkin*-related mitochondrial autophagy, leading to liver steatosis and inflammation. Numerous mitophagy-network genes, such as *Parkin*, *Atg5*, *Tom20*, *LC3* and *Lamp2*, are detected under nutrient deprivation [63]. Similarly, we found that SELENOM deficiency suppressed nutrient starvation-induced mitophagy, while SELENOM overexpression effectively rescued the PA-induced mitophagy impairment, suggesting that SELENOM sustains *Parkin*-related mitophagy activation to decrease hepatocyte apoptosis. Thus, SELENOM is a key activator that mediates the hepatic network involved in *Parkin*-related mitophagy to maintain liver function.

The activation of *AMPK/MFN2* maintains the biological function of mitochondria to regulate the process of energy metabolism [64]. Several previous studies have shown that *AMPK* could regulate the metabolic impact of pro-inflammatory cytokine and lipogenic genes expression through improvements in mitochondrial biogenesis [65]. Consistent with this, deletion of SELENOM promote the obesity-induced increase lipogenic genes expression in liver via affecting *AMPKα1–MFN2* pathway, which also includes increased expression of pro-inflammatory genes involved in NAFLD. Several pieces of evidence indicate a close relationship between *AMPKα1* function and *Parkin*-related mitophagy [66]. The regulation of mitophagy by energy stress is related to *AMPKα1* and *MFN2*, and *AMPKα1* regulates the autophagic ability of mouse embryonic fibroblasts via direct interaction with *MFN2* [27]. In the present study, we show that the level of *AMPKα1* phosphorylation was significantly suppressed in SELENOM-deficient livers in response to HFD treatment along with impaired mitophagy induction. Mechanistically, PA treatment led to the decrease in *AMPKα1* phosphorylation and reduced mitophagy, which was abolished SELENOM overexpression. Importantly, *AMPKα1* inhibition by Compound C ameliorated the effect of SELENOM, suggesting that SELENOM mediates mitophagy in an *AMPKα1*-dependent manner. Our study demonstrated that SELENOM could promote *Parkin*-related mitophagy via interacting with the *AMPKα1–MFN2* signal pathway to impede NAFLD development. In addition, the multiple roles of signaling pathways mediated by the *SELENOM–AMPKα1–MFN2* axis in the pathogenesis of liver diseases need to be further studied.

Conclusions

In conclusion, our findings show that energy stress-induced downregulation of SELENOM in hepatocytes could aggravate HFD-mediated liver damage. SELENOM deficiency increased oxidative stress, mitochondrial apoptosis, inflammation, steatosis, and fibrosis in HFD-treated livers. SELENOM enhanced *Parkin*-mediated mitophagy induced by energy stress via activation of the *AMPKα1–MFN2* pathway to prevent the pathogenesis of NAFLD. Our findings highlight SELENOM as a molecular target of NAFLD pathogenesis and reveal the importance of SELENOM and *Parkin*-mediated mitophagy in maintaining mitochondrial homeostasis in hepatocytes.

Supplementary Information The online version contains supplementary material available at https://doi.org/10.1007/s00018-022-04385-0.

Author contributions JC designed the study and JH wrote the manuscript. JY is the guarantor of this work. XC, HZ and YZ researched data and helped design experiments. QL and ZZ takes responsibility for the integrity of the data and helped design experiments. All authors have read the manuscript and agreed to submit it in its current form for consideration for publication in the Journal.

Funding This study was supported by the National Natural Science Foundation of China (31872531).

Availability of data and materials All data generated or analyzed during this study are included in this published article.

Declarations

Conflict of interest The authors declare that they have no competing interests.

Ethics approval and consent to participate Animal experiments in our study were subject to ethical review by the Animal Care and Use Committee of Northeast Agricultural University (SRM-11), Harbin, China. The investigation conforms to directive 2010/63/EU of the European parliament. All authors agreed to participate.

Consent for publication All authors read the manuscript and agreed to submission.

References

1. Polyzos SA, Kountouras J, Goulas A, Duntas L (2020) Selenium and selenoprotein P in nonalcoholic fatty liver disease. Hormones (Athens) 19:61–72. https://doi.org/10.1007/s42000-019-00127-3
2. Qiao L, Men L, Yu S et al (2022) Hepatic deficiency of selenoprotein S exacerbates hepatic steatosis and insulin resistance. Cell Death Dis 13:275. https://doi.org/10.1038/s41419-022-04716-w
3. Guerriero E, Accardo M, Capone F, Colonna G, Castello G, Costantini S (2014) Assessment of the Selenoprotein M (SELM) over-expression on human hepatocellular carcinoma tissues by immunohistochemistry. Eur J Histochem 58:2433. https://doi.org/10.4081/ejh.2014.2433
4. Zhou JC, Zhao H, Tang JY, Li JG, Liu XL, Zhu YM (2011) Molecular cloning, chromosomal localization and expression profiling of porcine selenoprotein M gene. Genes Genomics 33:529. https://doi.org/10.1007/s13258-010-0127-1
5. Gong T, Hashimoto AC, Sasuclark AR, Khadka VS, Gurary A, Pitts MW (2019) Selenoprotein M Promotes Hypothalamic Leptin Signaling and Thioredoxin Antioxidant Activity. Antioxid Redox Signal. https://doi.org/10.1089/ars.2018.7594
6. Ferguson AD, Labunskyy VM, Fomenko DE et al (2006) NMR structures of the selenoproteins Sep15 and SelM reveal redox activity of a new thioredoxin-like family. J Biol Chem 281:3536–3543. https://doi.org/10.1074/jbc.M511386200
7. Chen P, Wang RR, Ma XJ, Liu Q, Ni JZ (2013) Different forms of Selenoprotein M differentially affect Aβ aggregation and ROS generation. Int J Mol Sci 14:4385–4399. https://doi.org/10.3390/ijms14034385
8. Reeves MA, Bellinger FP, Berry MJ (2010) The neuroprotective functions of selenoprotein M and its role in cytosolic calcium regulation. Antioxid Redox Signal 12:809–818. https://doi.org/10.1089/ars.2009.2883
9. Addinsall AB, Wright CR, Andrikopoulos S, van der Poel C, Stupka N (2018) Emerging roles of endoplasmic reticulum-resident selenoproteins in the regulation of cellular stress responses and the implications for metabolic disease. Biochem J 475:1037–1057. https://doi.org/10.1042/bcj20170920
10. Wang P, Lu Z, He M, Shi B, Lei X, Shan A (2020) The effects of endoplasmic-reticulum-resident Selenoproteins in a nonalcoholic fatty liver disease pig model induced by a high-fat diet. Nutrients. https://doi.org/10.3390/nu12030692
11. Ma YM, Guo YZ, Ibeanu G et al (2017) Overexpression of selenoprotein H prevents mitochondrial dynamic imbalance induced by glutamate exposure. Int J Biol Sci 13:1458–1469. https://doi.org/10.7150/ijbs.21300
12. Day K, Seale LA, Graham RM, Cardoso BR (2021) Selenotranscriptome network in non-alcoholic fatty liver disease. Front Nutr 8:744825. https://doi.org/10.3389/fnut.2021.744825
13. Pitts MW, Reeves MA, Hashimoto AC et al (2013) Deletion of selenoprotein M leads to obesity without cognitive deficits. J Biol Chem 288:26121–26134. https://doi.org/10.1074/jbc.M113.471235
14. Musso G, Cassader M, Paschetta E, Gambino R (2018) Bioactive lipid species and metabolic pathways in progression and resolution of nonalcoholic Steatohepatitis. Gastroenterology 155:282–302. https://doi.org/10.1053/j.gastro.2018.06.031 (**e288**)
15. Ortiz M, Soto-Alarcón SA, Orellana P et al (2020) Suppression of high-fat diet-induced obesity-associated liver mitochondrial dysfunction by docosahexaenoic acid and hydroxytyrosol co-administration. Dig Liver Dis 52:895–904. https://doi.org/10.1016/j.dld.2020.04.019
16. Nageeb MM, Khatab MI, Abdel-Sameea AA, Teleb NA (2020) Adelmidrol protects against non-alcoholic steatohepatitis in mice. Naunyn Schmiedebergs Arch Pharmacol 393:777–784. https://doi.org/10.1007/s00210-019-01785-1
17. Aqel B, DiBaise JK (2015) Role of the Gut microbiome in nonalcoholic fatty liver disease. Nutr Clin Pract 30:780–786. https://doi.org/10.1177/0884533615605811
18. Simões ICM, Fontes A, Pinton P, Zischka H, Wieckowski MR (2018) Mitochondria in non-alcoholic fatty liver disease. Int J Biochem Cell Biol 95:93–99. https://doi.org/10.1016/j.biocel.2017.12.019
19. Zhao H, Wang Y, Liu Y et al (2021) ROS-induced hepatotoxicity under Cypermethrin: involvement of the crosstalk between Nrf2/Keap1 and NF-κB/iκB-α pathways regulated by proteasome. Environ Sci Technol 55:6171–6183. https://doi.org/10.1021/acs.est.1c00515
20. Palikaras K, Lionaki E, Tavernarakis N (2015) Coordination of mitophagy and mitochondrial biogenesis during ageing in *C. elegans*. Nature 521:525–528. https://doi.org/10.1038/nature14300
21. Qiu YN, Wang GH, Zhou F et al (2019) PM2.5 induces liver fibrosis via triggering ROS-mediated mitophagy. Ecotoxicol Environ Saf 167:178–187. https://doi.org/10.1016/j.ecoenv.2018.08.050
22. Fan RF, Tang KK, Wang ZY, Wang L (2021) Persistent activation of Nrf2 promotes a vicious cycle of oxidative stress and autophagy inhibition in cadmium-induced kidney injury. Toxicology 464:152999. https://doi.org/10.1016/j.tox.2021.152999
23. Wu M, Chen P, Liu F et al (2021) ONX0912, a selective oral proteasome inhibitor, triggering mitochondrial apoptosis and mitophagy in liver cancer. Biochem Biophys Res Commun 547:102–110. https://doi.org/10.1016/j.bbrc.2021.02.037
24. Yamada T, Murata D, Adachi Y et al (2018) Mitochondrial stasis reveals p62-mediated ubiquitination in Parkin-independent Mitophagy and Mitigates Nonalcoholic fatty liver disease. Cell Metab 28:588-604.e585. https://doi.org/10.1016/j.cmet.2018.06.014
25. Wang H, Ni HM, Chao X et al (2019) Double deletion of PINK1 and Parkin impairs hepatic mitophagy and exacerbates acetaminophen-induced liver injury in mice. Redox Biol 22:101148. https://doi.org/10.1016/j.redox.2019.101148
26. He L, Zhou Q, Huang Z et al (2019) PINK1/Parkin-mediated mitophagy promotes apelin-13-induced vascular smooth muscle

cell proliferation by AMPKα and exacerbates atherosclerotic lesions. J Cell Physiol 234:8668–8682. https://doi.org/10.1016/j.ceb.2015.01.002
27. Hu Y, Chen H, Zhang L et al (2021) The AMPK-MFN2 axis regulates MAM dynamics and autophagy induced by energy stresses. Autophagy 17:1142–1156. https://doi.org/10.1080/15548627.2020.1749490
28. Seabright AP, Fine NHF, Barlow JP et al (2020) AMPK activation induces mitophagy and promotes mitochondrial fission while activating TBK1 in a PINK1-Parkin independent manner. Faseb J 34:6284–6301. https://doi.org/10.1096/fj.201903051R
29. Zhang R, Chu K, Zhao N et al (2019) Corilagin alleviates nonalcoholic fatty liver disease in high-fat diet-induced C57BL/6 mice by ameliorating oxidative stress and restoring autophagic flux. Front Pharmacol 10:1693. https://doi.org/10.3389/fphar.2019.01693
30. Kumar S, Verma AK, Rani R et al (2020) Hepatic deficiency of augmenter of liver regeneration predisposes to nonalcoholic Steatohepatitis and fibrosis. Hepatology 72:1586–1604. https://doi.org/10.1002/hep.31167
31. Wan J, Zhang Y, Yang D et al (2021) Gastrodin improves nonalcoholic fatty liver disease via activation of the AMPK signaling pathway. Hepatology. https://doi.org/10.1002/hep.32068
32. Zhang Y, Xu Y, Chen B, Zhao B, Gao XJ (2021) Selenium deficiency promotes oxidative stress-induced mastitis via activating the NF-κB and MAPK pathways in dairy cow. Biol Trace Elem Res. https://doi.org/10.1007/s12011-021-02882-0
33. Song N, Wang W, Wang Y, Guan Y, Xu S, Guo MY (2021) Hydrogen sulfide of air induces macrophage extracellular traps to aggravate inflammatory injury via the regulation of miR-15b-5p on MAPK and insulin signals in trachea of chickens. Sci Total Environ 771:145407. https://doi.org/10.1016/j.scitotenv.2021.145407
34. Momcilovic M, Shirihai O, Murphy MP, Koehler CM, Sadeghi S, Shackelford DB (2020) Reply to: in vivo quantification of mitochondrial membrane potential. Nature 583:E19-e20. https://doi.org/10.1038/s41586-020-2367-9
35. Miao Z, Miao Z, Shi X, Wu H, Yao Y, Xu S (2022) The antagonistic effect of selenium on lead-induced apoptosis and necroptosis via P38/JNK/ERK pathway in chicken kidney. Ecotoxicol Environ Saf 231:113176. https://doi.org/10.1016/j.ecoenv.2022.113176
36. Novoselov SV, Kryukov GV, Xu XM, Carlson BA, Hatfield DL, Gladyshev VN (2007) Selenoprotein H is a nucleolar thioredoxin-like protein with a unique expression pattern. J Biol Chem 282:11960–11968. https://doi.org/10.1074/jbc.M701605200
37. Zheng Y, Guan H, Yang J, Cai J, Liu Q, Zhang Z (2021) Calcium overload and reactive oxygen species accumulation induced by selenium deficiency promote autophagy in swine small intestine. Anim Nutr 7:997–1008. https://doi.org/10.21203/rs.3.rs-118703/v1
38. Chi Q, Hu X, Liu Z, Han Y, Li S (2021) H2S exposure induces cell death in the broiler thymus via the ROS-initiated JNK/MST1/FOXO1 pathway. Ecotoxicol Environ Saf 222:112488. https://doi.org/10.1016/j.ecoenv.2021.112488
39. Liu XJ, Wang YQ, Shang SQ, Xu S, Guo M (2022) TMT induces apoptosis and necroptosis in mouse kidneys through oxidative stress-induced activation of the NLRP3 inflammasome. Ecotoxicol Environ Saf 230:113167. https://doi.org/10.1016/j.ecoenv.2022.113167
40. Schuster S, Cabrera D, Arrese M, Feldstein AE (2018) Triggering and resolution of inflammation in NASH. Nat Rev Gastroenterol Hepatol 15:349–364. https://doi.org/10.1038/s41575-018-0009-6
41. Chen X, Bi M, Yang J et al (2022) Cadmium exposure triggers oxidative stress, necroptosis, Th1/Th2 imbalance and promotes inflammation through the TNF-α/NF-κB pathway in swine small intestine. J Hazard Mater 421:126704. https://doi.org/10.1016/j.jhazmat.2021.126704
42. Sangineto M, Bukke VN, Bellanti F et al (2021) A novel nutraceuticals mixture improves liver Steatosis by preventing oxidative stress and mitochondrial dysfunction in a NAFLD model. Nutrients. https://doi.org/10.3390/nu13020652
43. Zhang HR, Zhao FQ, Gai XX et al (2022) Astilbin attenuates apoptosis induced by cadmium through oxidative stress in carp(Cyprinus carpio L.) head kidney lymphocyte. Fish Shellfish Immunol 13:S1050–4648. https://doi.org/10.1016/j.fsi.2022.05.021
44. Paech F, Abegg VF, Duthaler U, Terracciano L, Bouitbir J, Krähenbühl S (2018) Sunitinib induces hepatocyte mitochondrial damage and apoptosis in mice. Toxicology 409:13–23. https://doi.org/10.1016/j.tox.2018.07.009
45. Kruppa AJ, Buss F (2018) Actin cages isolate damaged mitochondria during mitophagy. Autophagy 14:1644–1645. https://doi.org/10.1080/15548627.2018.1486152
46. Wei Y, Pattingre S, Sinha S, Bassik M, Levine B (2008) JNK1-mediated phosphorylation of Bcl-2 regulates starvation-induced autophagy. Mol Cell 30:678–688. https://doi.org/10.1016/j.molcel.2008.06.001
47. Eiyama A, Okamoto K (2015) PINK1/Parkin-mediated mitophagy in mammalian cells. Curr Opin Cell Biol 33:95–101. https://doi.org/10.1016/j.ceb.2015.01.002
48. Park HS, Song JW, Park JH et al (2020) TXNIP/VDUP1 attenuates steatohepatitis via autophagy and fatty acid oxidation. Autophagy. https://doi.org/10.1080/15548627.2020.1834711
49. Gong T, Hashimoto AC, Sasuclark AR, Khadka VS, Gurary A, Pitts MW (2021) Selenoprotein M promotes hypothalamic Leptin signaling and Thioredoxin antioxidant activity. Antioxid Redox Signal 35:775–787. https://doi.org/10.1089/ars.2018.7594
50. Zhang ZH, Song GL (2021) Roles of Selenoproteins in brain function and the potential mechanism of selenium in Alzheimer's disease. Front Neurosci 15:646518. https://doi.org/10.3389/fnins.2021.646518
51. Qazi IH, Yang H, Wei S et al (2020) Dietary selenium deficiency and supplementation differentially modulate the expression of two ER-resident selenoproteins (selenoprotein K and selenoprotein M) in the ovaries of aged mice: preliminary data. Reprod Biol 20:441–446. https://doi.org/10.1016/j.repbio.2020.07.006
52. Gong T, Berry MJ, Pitts MW (2016) Selenoprotein M: structure, expression and functional relevance. Springer International Publishing. https://doi.org/10.1007/978-3-319-41283-2_21
53. Varlamova EG et al (2019) Protein partners of Selenoprotein SELM and the role of selenium compounds in regulation of its expression in human cancer cells. Dokl Biochem Biophys 488:300–303. https://doi.org/10.1134/S1607672919050065
54. Liu Q, Du P, Zhu Y, Zhang X, Cai J, Zhang Z (2022) Thioredoxin reductase 3 suppression promotes colitis and carcinogenesis via activating pyroptosis and necrosis. Cell Mol Life Sci 79:106
55. Li J, Zhang W, Zhou P, Tong X, Guo D, Lin H (2022) Selenium deficiency induced apoptosis via mitochondrial pathway caused by Oxidative Stress in porcine gastric tissues. Res Vet Sci 144:142–148. https://doi.org/10.1134/S1607672919050065
56. Chi Q, Luan Y, Zhang Y, Hu X, Li S (2019) The regulatory effects of miR-138-5p on selenium deficiency-induced chondrocyte apoptosis are mediated by targeting SelM. Metallomics 11:845–857. https://doi.org/10.1039/c9mt00006b
57. Gilkerson RW, De Vries RL, Lebot P et al (2012) Mitochondrial autophagy in cells with mtDNA mutations results from synergistic loss of transmembrane potential and mTORC1 inhibition. Hum Mol Genet 21:978–990. https://doi.org/10.1093/hmg/ddr529
58. Miao Z, Miao Z, Wang S, Wu H, Xu S (2022) Exposure to imidacloprid induce oxidative stress, mitochondrial dysfunction, inflammation, apoptosis and mitophagy via NF-kappaB/JNK pathway in grass carp hepatocytes. Fish Shellfish Immunol 120:674–685. https://doi.org/10.1016/j.fsi.2021.12.017

59. Tanaka M, Sato A, Kishimoto Y, Mabashi-Asazuma H, Kondo K, Iida K (2020) Gallic acid inhibits lipid accumulation via AMPK pathway and suppresses apoptosis and macrophage-mediated inflammation in hepatocytes. Nutrients. https://doi.org/10.3390/nu12051479
60. Tanaka S, Hikita H, Tatsumi T et al (2016) Rubicon inhibits autophagy and accelerates hepatocyte apoptosis and lipid accumulation in nonalcoholic fatty liver disease in mice. Hepatology 64:1994–2014. https://doi.org/10.1002/hep.28820
61. Reinartz A, Ehling J, Leue A et al (2010) Lipid-induced up-regulation of human acyl-CoA synthetase 5 promotes hepatocellular apoptosis. Biochim Biophys Acta 1801:1025–1035. https://doi.org/10.1016/j.bbalip.2010.04.010
62. Wen F, Shi Z, Liu X et al (2021) Acute elevated resistin exacerbates mitochondrial damage and aggravates liver Steatosis through AMPK/PGC-1α signaling pathway in male NAFLD mice. Horm Metab Res 53:132–144. https://doi.org/10.1055/a-1293-8250
63. Singh R, Kaushik S, Wang Y et al (2009) Autophagy regulates lipid metabolism. Nature 458:1131–1135. https://doi.org/10.1038/nature07976
64. Dong H, Zhou W, Xin J et al (2019) Salvinorin A moderates postischemic brain injury by preserving endothelial mitochondrial function via AMPK/Mfn2 activation. Exp Neurol 322:113045. https://doi.org/10.1016/j.expneurol.2019.113045
65. Lyons CL, Roche HM (2018) Nutritional Modulation of AMPK-Impact upon Metabolic-Inflammation. Int J Mol Sci. https://doi.org/10.3390/ijms19103092
66. Mihaylova MM, Shaw RJ (2011) The AMPK signalling pathway coordinates cell growth, autophagy and metabolism. Nat Cell Biol 13:1016–1023. https://doi.org/10.1038/ncb2329